Ab initio simulation of the metal/nonmetal transition in expanded fluid mercury

G. Kresse and J. Hafner
Institut für Theoretische Physik and Center for Computational Materials Science, Technische Universität Wien, Wiedner Hauptstrasse 8-10, A-1040 Wien, Austria
(Received 5 November 1996)

We present an investigation of the variation of the structural and electronic properties of liquid mercury for states along the liquid-vapor coexistence line, spanning the range from the triple point to the critical point. Our study is based on *ab initio* density-functional molecular dynamics on the Born-Oppenheimer surface. Of central interest is the metal/nonmetal transition occurring at densities approximately twice the critical densities. We show that the density-functional calculations describe the atomic structure very accurately over the entire range from the triple point to the critical point. We find that a single-particle gap between the 6*s* and the 6*p* band opens at a density of about 8.8 g cm^{-3}, i.e., very close to the density where optical measurements locate the onset of the formation of an optical gap. The detailed investigation of the band edges and of the participation ratio of the eigenstates suggests that the metal/nonmetal transition is best described as a simple band-crossing transition and that electron localization and many-body effects may not be as important as assumed in current scenarios for the transition. [S0163-1829(97)06311-X]

I. INTRODUCTION

The investigation of the properties of liquid metals, expanded by heating up to the liquid-vapor critical point, has attracted much attention over the past decades.[1] The main objectives of this work are to study how the physical properties vary under changes of the density that are large enough to transform the liquid metal into a nonmetal through large expansion, to find out whether the metal/nonmetal (M/NM) transition occurs at sub- or supercritical conditions and to establish a microscopic scenario for this transition. Because liquid mercury possesses a low critical temperature and pressure, the M/NM transition has been studied experimentally in great detail through measurements of the electrical conductivity, thermopower, Hall coefficient, optical reflectivity and absorption, nuclear magnetic resonance, atomic structure, sound velocity, and equation of state.[2–10] In particular it has been pointed out that the M/NM transition also influences the critical behavior and leads to a violation of the ''law of rectilinear diameters'' for the liquid-vapor coexistence curve.[8] The possibility that this law (which is rather an empirical rule for simple insulating fluids) could be violated for systems where the interatomic interactions depend strongly on the thermodynamic state (like for liquid metals close to a M/NM transition) had been anticipated by a number of theoretical studies.[11–14] For expanded Hg, where in contrast to the expanded alkali metals the *s*-*p* band gap opens at higher than critical densities, the high-density side of the coexistence curve is much steeper than in the alkali metals, reflecting the interplay of the M/NM and liquid/vapor transitions.[8] For liquid Hg a thermodynamic two-state model admitting the coexistence of neutral Hg atoms and screened Hg^+ and Hg^{2+} ions and allowing for association processes leading to the formation of neutral Hg_2 dimers and molecular Hg_2^+ and Hg_2^{2+} ions accounts, in a semiquantitative way, for the form of the coexistence curve.[15,16] For the M/NM transition this leads to a scenario associating the M/NM transition with the clustering of Hg ions forming a dense metallic network and the decreasing size and concentration of these clusters.[15] However, this is essentially an atomic model and does not offer a microscopic description of the electronic transition.

Hence, in spite of the wealth of experimental information available, the nature of the M/NM transition is still insufficiently understood. Although there is general agreement that within the Bloch-Wilson band model this type of transition has to be expected in any divalent metal when the expansion is sufficiently large so that the *s* and *p* conduction bands no longer overlap, very different scenarios have been proposed for the mechanism of the transition. Mott[17] proposed that the general features of the band model will remain valid in the liquid state, but with the band edges smeared out by disorder and the band tails overlapping in the region of the Fermi energy E_F. Hence the real gap is replaced by a minimum in electronic density of states (DOS) or pseudogap. States in the pseudogap will be localized due to disorder (Anderson localization) and the M/NM transition arises from the formation of a mobility gap within the pseudogap. An optical gap is expected to open only at densities that are even lower than those at the M/NM transition. But when the variation of the DOS is driven by changes in the density, large fluctuations in the density such as those that occur close to the critical point must play an important role. This has led Cohen and Jortner[18] to propose a semiclassical percolation model for the M/NM transition based on the assumption of the simultaneous existence of metallic and semiconducting regions. While these two models are based on one-electron pictures, the correlation between density-fluctuations and the many-body aspect of the transition has been emphasized by Turkevich and Cohen.[19] They argued that the insulating expanded liquid mercury and the dense vapor constitute a disordered, inhomogeneous insulator phase. A correlation gap caused by the condensation of Frenkel excitons opens before a single-particle gap. A single-particle gap is expected to form only at the liquid-vapor critical point. The correlation gap becomes the single-particle gap only in the transition

regime from the excitonic insulator phase to the insulating vapor.

One of the motivations for the formulation of the excitonic insulator model was certainly the fact that band-structure calculations for expanded crystalline mercury in various structures with a fixed interatomic distance and decreasing coordination numbers indicated that the band gap opens only close to the critical density and not at the much higher density where the M/NM transition has been observed.[20–22] However, such calculations completely ignore all aspects of disorder. The form of the electronic DOS close to the Fermi level depends strongly on the crystalline structure [simple, body-centered-cubic (bcc), and face-centered cubic (fcc), and diamond (dia)] used to model the liquid structure. The low-coordinated simple cubic ($N_c=6$) and diamond ($N_c=4$) structures (which should be most representative for the expanded metals) in particular show a rather contrasting behavior: For the diamond structure E_F falls very close to the lower edge of a sharp peak in the p-state DOS, whereas in the simple cubic structure E_F falls into a region of high DOS. Hence the variation of the DOS at E_F in a series of fcc-bcc-sc-dia calculations with a fixed nearest-neighbor distance reflects rather the effect of the changing long-range structural correlations than the effect of a homogeneous expansion of the fluid. An attempt to calculate the DOS for liquid Hg over a wide range of densities was made by Yonezawa *et al.*[23] on the basis of a tight-binding single-site-scattering approximation. The onset of an energy gap was found only at densities in the range $2-4$ g/cm^3, i.e., at densities even lower than predicted by the crystalline band-structure calculations and much lower than the critical density. Recent self-consistent supercell calculations of the electronic DOS based on realistic models for liquid Hg (Ref. 24) predict a shallow minimum in the DOS close to the Fermi level and are in good agreement with photoemission studies.[25] However, both theory and experiment refer only to densities close to the triple point.

Simultaneous self-consistent calculations of the atomic and the electronic structure of disordered materials are now possible using the *ab initio* density-functional molecular-dynamics (MD) techniques pioneered by Car and Parrinello (CP).[26] However, it has turned out that while the fictitious Lagrangian dynamics for the electronic degrees of freedom proposed by CP is well suited for semiconducting systems, the nonadiabaticity problems are much more difficult to handle for metals. Here it is more advantageous to perform MD *on the Born-Oppenheimer surface*, calculating the electronic ground state and the Hellmann-Feynman forces exactly after each move of the ions.[27–29] Still, mercury is very difficult to handle since the strong hybridization of the s and d states makes it necessary to treat all twelve s and d electrons dynamically. The fast dynamics at high temperatures close to the critical point leads to further massive computational difficulties.

In this paper we present an *ab initio* MD study of the structural and electronic properties of fluid mercury for a series of states along the liquid/vapor coexistence curve, spanning the range from close to the triple point to the critical point. In our calculations all ten $5d$ and the two $6s,p$ electrons are treated as valence electrons. Our results for the atomic structure are in very good agreement with the most recent x-ray-diffraction experiments;[9] the calculated DOS's show that a single-particle gap opens at precisely the same density where recent optical absorption data[6] locate the onset of an optical gap. The analysis of the electronic eigenstates suggests that the scenario for the M/NM transitions is simpler than those advocated to date: *at least for the system size we used* we cannot find any indication for a disorder-induced tailing of the band edges or for the onset of localization near the Fermi edge. There is no distinction between a mobility gap and the optical gap. This suggests the conclusion that the M/NM transition in expanded fluid mercury arises from the formation of a single-particle gap between the s and p bands as the bands become narrower with decreasing coordination number, but is not directly related to disorder-induced localization. However, we have to remember the limitations inherent in our approach: the well-known tendency of the local-density approximation to underestimate the width of the gap and the limited system-size that can be handled in *ab initio* calculations. A critical discussion of these effects is given in Sec. VI.

II. AB INITIO LOCAL-DENSITY MOLECULAR DYNAMICS

Our calculations have been performed using the Vienna *ab initio* simulation program (VASP).[28–31] The VASP is based on the following principles.

(i) *Finite-temperature local-density functional theory* leads to a smearing of the one-electron levels and to a fractional occupancy of states close to the Fermi edge. The smearing improves the convergence of the $\vec{k}$-space integrals; the fractional occupancy is important for achieving a good stability of the simulations (exact conservation of the free energy) even in metallic systems. In practice we use the smearing functions proposed by Methfessel and Paxton.[32]

(ii) *The exact Kohn-Sham ground state is calculated after each ionic move* via a sequential band-by-band algorithm based on the minimization of the norm of the residual vector to each eigenstate and on an efficient charge-density mixing.[30,31]

(iii) The electron-ion interaction is described by *ultrasoft pseudopotentials* similar to those proposed by Vanderbilt.[33,34] This is important for achieving a reasonable plane-wave convergence even for the relatively localized $5d$ electrons. We used two nonlocal projectors (i.e., two reference energies) per angular-momentum component, the cutoff radii are $R_{c,l}=3.2$ a.u. for $l=2$ and $R_{c,1}=R_{c,0}=3.0$ a.u for $l=1,0$; the radii for the calculation of the augmentation functions are $R_{\mathrm{aug},2}=3.0$ a.u. and $R_{\mathrm{aug},1}=R_{\mathrm{aug},0}=2.9$ a.u. The truncated all-electron pseudopotential has been chosen as the local component. With this choice of the pseudopotential, good plane-wave convergence can be achieved with a cutoff energy of $E_{\mathrm{cut}}=150$ eV. The pseudopotential has been carefully tested in calculations of the Hg_2 dimer and of the crystal structures (see the next section).

(iv) The MD simulations have been performed in the *canonical ensemble*, using Nosé dynamics and a fourth-order predictor-corrector algorithm for the integration of the equations of motion. For all further details of the technique, see Refs. 29 and 30.

III. THE Hg DIMER

For the Hg_2 dimer we calculate a bond length of $d_0 = 3.058$ Å, a binding energy of $E_B = 0.207$ eV, and a molecular eigenfrequency of $\omega = 53.9$ cm^{-1}, to be compared with the experimental values of $d_0 = 3.63$ Å and $E_B = 0.07$ eV.[35] Our results are in good agreement with earlier local-density-functional (LDF) calculations by Ballone and Galli,[36] but in admittedly rather modest agreement with experiment. For the group-II dimers the overbinding tendency of the local-density approximation is notorious and well documented in the literature (see Ref. 36 for a more detailed discussion). Calculations using a generalized gradient approximation (GGA) (we used the functional proposed by Perdew *et al.*[37]) show a drastic improvement over the LDF results: the bond length ($d_0 = 3.533$ Å) and binding energy ($E_B = 0.067$ eV) are now in almost perfect agreement with experiment. However, we have to note that the degree of agreement is to some degree fortuitous. For most metal dimers the GGA does not lead to a complete compensation of the LDF error (see also below).

IV. ATOMIC AND ELECTRONIC STRUCTURE OF THE CRYSTALLINE PHASES OF Hg

We have also investigated the phase stability of solid Hg. At ambient temperature the experimentally stable crystalline structure may be described as a rhombohedral distortion of the fcc structure (α-Hg), whereas under pressure and at zero temperature the stable crystalline configuration is a tetragonal distortion of the bcc structure (β-Hg).[38,39] Figure 1 shows the variation of the total energy of crystalline Hg as a function of a rhombohedral distortion of the fcc lattice (the distortion parameter α measures the contraction/expansion along the body diagonal) and as a function of a tetragonal distortion of a bcc lattice (the distortion parameter is equal to the axial ratio c/a). At each given distortion, the volume was relaxed so that the zero-pressure equilibrium condition is satisfied. We find that for both the α and β phases the equilibrium structure (i.e., the parameters α and c/a describing the distortion) and volume are predicted with good accuracy (see Table I). Figure 2 shows the variation of the total energy and pressure of the α- and β-phases and of a hexagonal-close-packed phase (which is the high-pressure δ-Hg phase according to Schulte and Holzapfel.)[38] At each volume the structural parameters have been optimized. Figure 3 shows the variation of the rhombohedral and tetrahedral distortions under compression or expansion. Whereas the rhombohedral distortion changes all the way from $\alpha = 0.5$ (i.e., a simple cubic structure) at a slight expansion to $\alpha = 1$ (i.e., a face-centered-cubic structure) at very high compression, the tetragonal distortion shows only little variation over a wide range of pressures. For the structural energy differences, the slightly disappointing result is that at zero temperature α-Hg is predicted to be more stable that β-Hg, in contradiction to the accepted phase diagram showing that β-Hg becomes the stable phase below $T \simeq 70$ K. From Fig. 2 it can be estimated that β-Hg should be lowered by about 10 meV/atom to bring the E-V curves in nearly perfect agreement with the experimental phase diagram. To rule out any possible errors, the calculations have been done with great care and high accuracy (i.e., a $15\times15\times15$ k point mesh and a 300-eV plane-wave cutoff), so that the overall accuracy is better than 1 meV. In addition, we have checked our results with an accurate norm-conserving pseudopotential (which required a cutoff of more than 800 eV) and obtained virtually the same results. The discrepancy between theory and experiment can be tentatively attributed to two rather different effects. (a) The vibrational contributions to the free energy

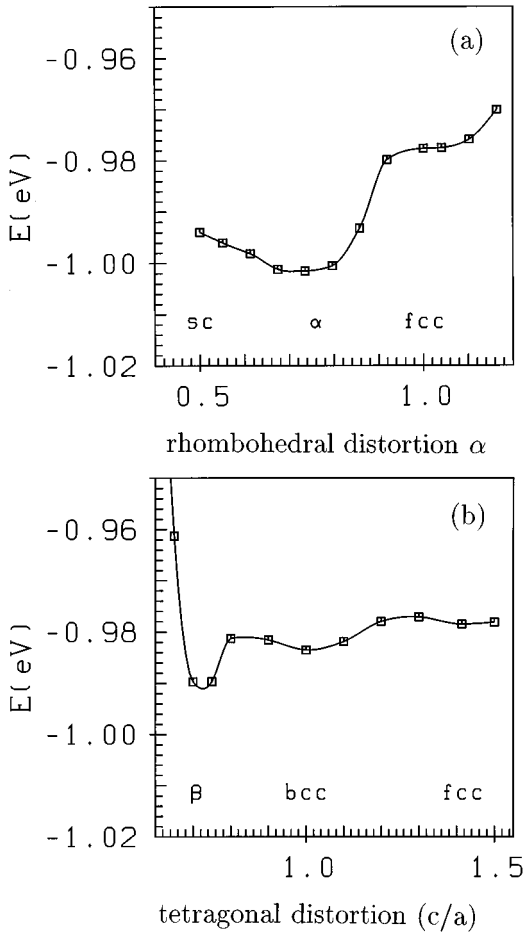

FIG. 1. Total energy as a function of the lattice distortion (a) α in the rhombohedral α-Hg and (b) c/a in the tetragonal β-Hg phases. For the definition of the distortion parameters, see the text.

TABLE I. Structural parameters for α-Hg and β-Hg: atomic volume V, bulk modulus B (the bulk modulus has been obtained by a full relaxation of the internal degrees of freedom, i.e., relaxation of α, at each volume), cohesive energy E, and parameters α and c/a which describes the distortion with respect to the fcc structure (for α-Hg) and the bcc structure (for β-Hg), respectively.

	V (Å^3)	B (kbar)	E	α
α-Hg (theory)	22.91	270	-1.002	0.76
α-Hg (experiment)	23.16[a]			0.79[b]
	V (Å^3)	B (kbar)	E	c/a
β-Hg (theory)	22.20	514	-0.991	0.716
β-Hg (experiment)	22.56[b]			0.707[b]

[a]Reference 39.
[b]Reference 47.

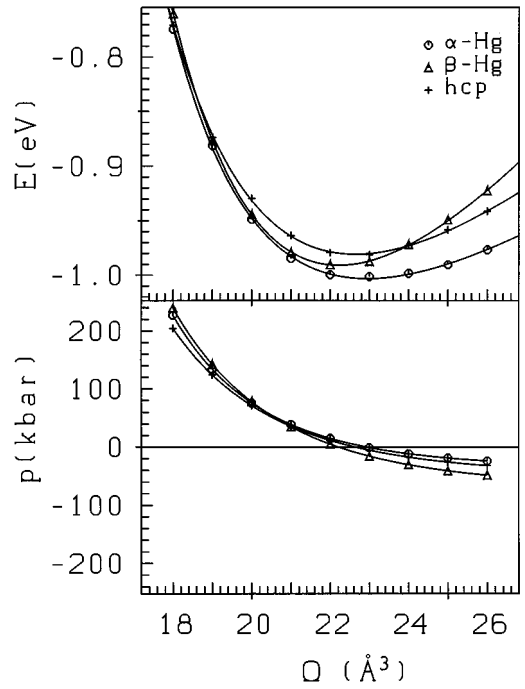

FIG. 2. Energy E and pressure p vs volume V for solid Hg in the α-Hg, β-Hg, and hexagonal-close-packed (hcp) structures.

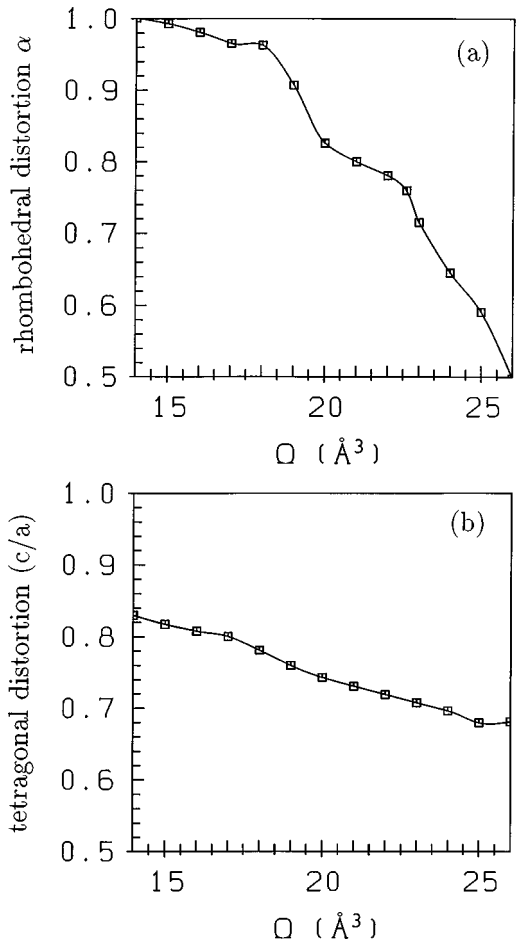

FIG. 3. Variation of the rhombohedral and tetragonal lattice distortions in (a) α-Hg and (b) β-Hg under compression/expansion; see the text.

are neglected. Our results for the bulk modulus show that the β phase is much harder than the α phase, so that the vibrational entropy should favor rather the ''soft'' α phase. However, one should keep in mind that both phases are rather anisotropic, so that it cannot be excluded that soft shear modes reverse the argumentation. Evidently, detailed studies of the vibrational properties (by both theory and experiment) would be of great interest. (b) The error stems from one of the basic approximations. We are currently using the LDF approximation, the neglect of spin-orbit coupling, and the frozen-core approximation. Because the ultrasoft pseudopotentials mimic the exact all-electron density with great accuracy, errors due to the pseudopotential approximation are negligible and the frozen-core approximation should also play only a minor rule for Hg. The calculations are also well converged with respect to the plane-wave cutoff. Even a calculation with a cutoff of only 150 eV reproduces the structural energy differences obtained with the hard norm-conserving pseudopotential to within $\sim$ 1 meV/atom. Nonlocal corrections could play a certain role. However, at the level of the GGA, we find that the corrections lead to a large increase of the equilibrium volume. This is in agreement with a general tendency of the GGA to ''overcorrect'' the LDA errors that we have found also in other heavy B-group elements (Sb, Bi, Te, etc.).[40,41] This leaves relativistic effects. Indeed, spin-orbit coupling leads to a splitting of the d band with the result that only the upper part overlaps with the s,p band so that the (s,p)-d hybridization eventually becomes anisotropic. Fully relativistic calculations will be necessary to settle this question.

Nevertheless, one should keep in mind that the error in the energy difference between the β and the α phase is very small ($\sim$ 100 K) and that all structural parameters of the α and the β phase show excellent agreement with experiment. We expect that the main source of error (i.e., the spin-orbit splitting of the d band) will be less important in the liquid phase because disorder will tend to intermix the two parts of the d band. One should also keep in mind that the maximum error is very small compared to the thermal energies.

Finally, we show in Fig. 4 the total and partial electronic densities of states of the equilibrium α- and β-Hg phases. In agreement with earlier calculations, we find a total bandwidth of $\sim$ 10 eV in both the α and β phases. The strong hybridization of s and p states with the d band extending from -9 eV to -6 eV binding energy induces a strong s resonance at the bottom of the band and a p resonance close to the center of gravity of the d band. s and p states are strongly intermixed in the upper part of the valence band. Just above the Fermi energy a structure-induced DOS minimum is found in both crystalline phases. The empty states above the DOS minimum are predominantly p like.

V. ATOMIC AND ELECTRONIC STRUCTURE OF EXPANDED LIQUID Hg

In our simulation of liquid Hg we considered ensembles of 50 atoms [i.e., $50 \times (10d+2s,p) = 600$ valence electrons] in a periodically repeated box at densities and temperatures

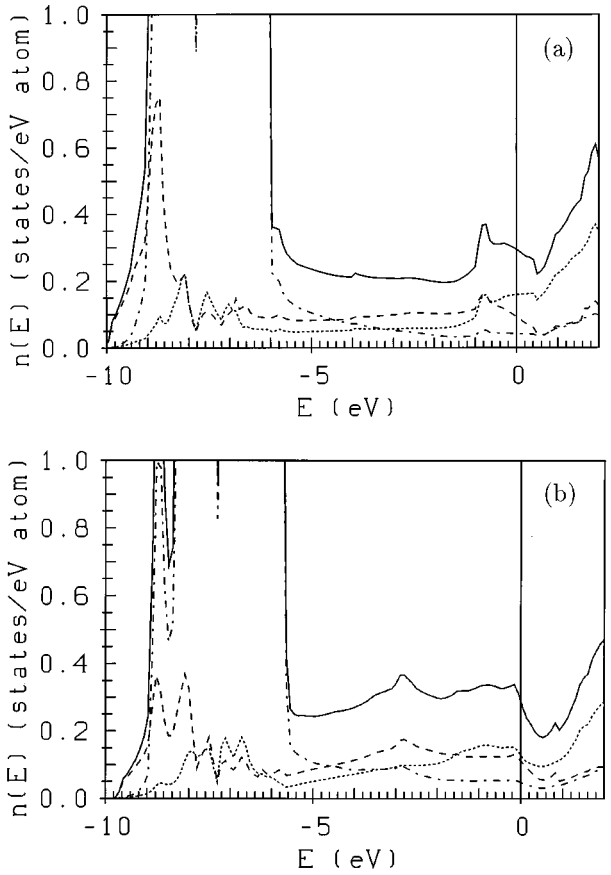

FIG. 4. Total and partial electronic densities of states (DOS) in the (a) α-Hg and (b) β-HG phases. Full line, total DOS; dashed, dotted, and dot-dashed lines, s, p, and d partial DOS's, respectively.

distributed along the coexistence line between the triple point ($\rho_t = 13.8$ g cm^{-3}) and the critical point ($\rho_c = 5.8$ g cm^{-3}, $T_c = 1751$ K). For the MD simulations, the forces have been calculated at one off-symmetry special $\vec{k}$ point (0.25,0.25,0.25), using first-order Methfessel-Paxton smearing with $\sigma = 0.1$ eV. In the following we describe the results obtained at $\rho = 12.40$ g cm^{-3} ($T = 773$ K), $\rho = 10.98$ g cm^{-3} ($T = 1273$ K), $\rho = 8.78$ g cm^{-3} ($T = 1723$ K), and $\rho = 5.80$ g cm^{-3} ($T = 1723$ K). The time-increment was chosen to be $\Delta t = 5$ fs at the highest density, and was stepwise reduced to $\Delta t = 3$ fs at the lowest density to account for the fast atomic motions. Each simulation was extended over about 3–4 ps.

A. Atomic structure

Figure 5(a) shows the variation of the pair-correlation correlation function $g(R)$, compared to the x-ray-diffraction data of Waseda.[42] We note a very good agreement between theory and experiment at all densities, but admittedly this is not a very stringent test because the experimental $g(R)$ is subject to rather large truncation errors. The important result is that the volume expansion of liquid Hg does not result in an increase of the mean interatomic distance R_1 (which remains almost unchanged up to the critical point), but in a decrease of the average coordination number N_c from nearly 10 to about 4; see Fig. 6 [note that the asymmetry of the first peak in $g(r)$ and the very shallow minimum separating the first from the second peak make a precise quantification of N_c very difficult; see the discussion in Ref. 9]. We also note that the decrease in the average coordination number is almost linear with density and that the fluctuations in the coordination number increase with decreasing density.

The static structure factor [Fig. 2(b)] is a more direct test of the predicted liquid structure. Again we note a very good agreement with experiment,[9] from low-Q vectors [where the increase of $S(Q)$ reflects the increasing importance of long-wavelength density fluctuations and the increasing compressibility] to the large-Q oscillations. Note that the $S(Q)$ data refer to the recent data of Tamura and Hosokawa,[9] while the $g(r)$ data shown in Fig. 2(a) refer to the older data of Waseda.[42] Unfortunately pair-correlation data based on the most recent experiments were not available. At the lowest density (which is very close to the critical point) we are able to observe the onset of critical density fluctuations. However, we should remember that due the limited size of our ensemble, we can observe fluctuations only up to a maximum correlation length of about 14 Å, corresponding to a smallest wave vector of 0.44 Å^{-1}. Still, the good agreement between the calculated and the measured structure factors down to this value shows that our simulations describe correctly not only short-range correlations, but also medium-range correlations extending to 3–4 interatomic distances.

Three-particle correlations are analyzed in Fig. 7 in the form of the distributions of the bond angles formed around a central atom as a function of the maximum length R_m of the bonds. At high densities, the bond angle distribution show two characteristic peaks at angles of $\theta \sim 60°$ and $\theta \sim 110°$, i.e., close to the bond angles in an icosahedron forming the dominant motif in a dense-random-packing structure. At lower densities the peak near 110° is gradually washed out, whereas the 60° peak subsists. This indicates that there are still quite well-defined short-range correlations in small clusters of a few atoms, whereas the very weak correlations between large bond angles indicate that large dense-packed metallic clusters disappear. This is also seen directly in snapshots of characteristic instantaneous configurations taken at different densities (Fig. 8): At high densities the entire system is strongly interconnected, forming a dense network of metallic bonds. At lower densities smaller closely packed regions alternate with low-density regions, conforming rather closely to the atomic scenario suggested for the M/NM transition.[15]

At densities close to the triple point the atomic structure calculated via the *ab initio* technique is in good agreement with classical molecular-dynamics simulations based on effective interatomic forces derived from pseudopotential perturbation theory.[24] However, whereas this nearly-free-electron approach breaks down already at densities higher than that of the M/NM transition (see, e.g., Ref. 16 for Hg and Ref. 43 for similar results for the expanded alkali metals), the *ab initio* calculations remain accurate up to the critical point. We take this as a first indication that the interatomic interactions are described correctly even in the regime of the M/NM transition.

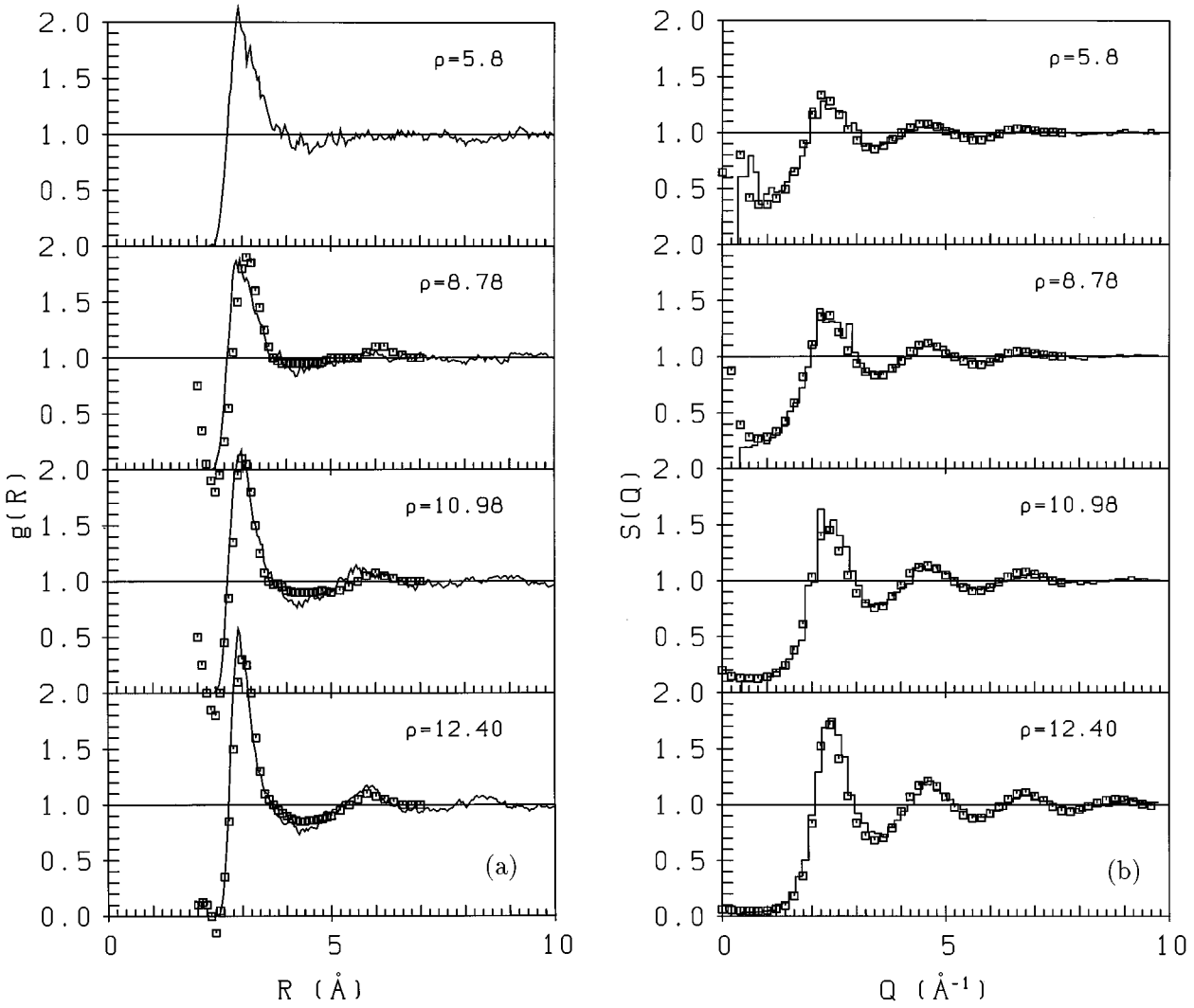

FIG. 5. (a) Pair correlation function $g(R)$ and (b) static structure factor $S(Q)$ of liquid mercury, calculated at four different states along the liquid/vapor coexistence curve. For each panel, the density ρ is given in g cm^{-3}. The full lines show the result of the *ab initio* simulations, the squares the x-ray-diffraction data of Tamura and Hosokawa (Ref. 9). All simulations have been performed for 50-atom ensembles.

B. Electronic density of states

Figure 9 shows the variation of the total and partial densities of states with decreasing density. The total DOS has been calculated for a series of states along the MD trajectory, using a larger $\vec{k}$ point set (four $\vec{k}$ points corresponding to a $4\times4\times4$ grid in the irreducible Brillouin zone of the simple cubic cell). The partial DOS's have been determined by projecting each plane-wave component of the eigenstates onto the spherical waves with $l=0,1,2$ inside the atomic spheres with radius 1.93 Å around each site.[44] Our results show that the 5*d* band overlaps strongly with the 6*s*,6*p* valence band. At the highest density, the calculated DOS is in good agreement with linear muffin-tin orbital supercell calculations[24] and with the photoemission intensities measured by Indlekofer *et al.* close to the triple point.[25] We also note that the DOS calculated for dense liquid Hg is very similar to that of the crystalline phases shown in Fig. 4. In the high-density melt, the *s*,*p* mixing in the occupied part of the valence band is even stronger than in the crystalline phases, but a demixing is observed at lower densities. The *s* and *p* resonances in the region of the *d* band are more symmetric in the liquid than in the solid and strongly reduced in the expanded melt. Close to the triple point theory and experiment predict a reduction of the DOS at E_F to about 80 % of its free-electron value. This is similar to the DOS at the Fermi level found in the crystalline phases. In our series we clearly recognize the gradual reduction of the DOS at E_F between $\rho = 12.4$ g cm^{-3} and $\rho = 8.8$ g cm^{-3} where a gap opens at the Fermi level (note that the edges of the gap tend to be obscured by the smearing of the one-electron levels, see also below). Extrapolating the optical absorption data measured in the range between $\rho = 4.3$ g cm^{-3} and $\rho = 7.5$ g cm^{-3} to higher densities Yao *et al.*[6] estimate that the single-particle gap opens first at a density of $\rho\sim$ 9–10 g cm^{-3}, in good agreement with estimates of the M/NM transition based on electronic transport data[5] and with our estimate of $\rho\sim$ 8.8 g cm^{-3}.

The density at which the gap at the Fermi level first appears depends very sensitively on the atomic structure. To

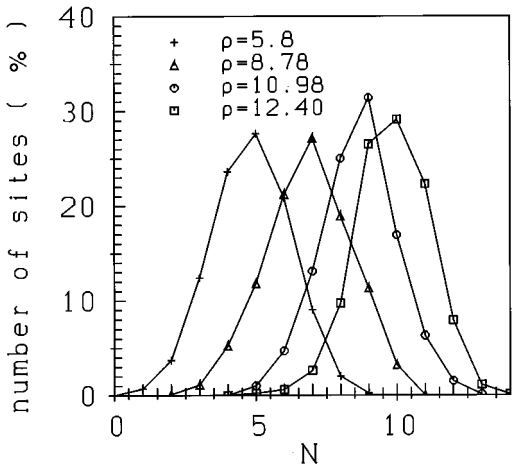

FIG. 6. Distribution of the nearest-neighbor coordination numbers at four different states along the liquid vapor coexistence curves. The density ρ is given in units of g cm^2.

show this, we have performed calculations for the fcc, bcc, sc, dia, and β-Hg structures at different densities. A gap at the Fermi level opens at a density of $\rho \sim 11$ g cm^{-3} for the fcc structure, at $\rho \sim 8.8$ g cm^{-3} for the bcc and β-Hg structures, and at $\rho \leqslant \rho_{\text{crit}}$ for the sc and dia structures. The important point is that for the structures with coordination numbers relatively close to that of the liquid, the gap opens only at densities that are much lower than for the liquid structure. Hence the disordered atomic arrangement is important for the formation of a band gap.

The width of the gap continues to increase up to the critical point. At the critical point the optical gap is $\Delta E \sim 1.8$ eV. The difference of the theoretical result of $\Delta E \sim 0.7$ eV corresponds to the usual trend of the local density approximation to underestimate the width of the gap. Note, however, that the failure of the LDA to predict the correct width of the gap has to be attributed to an inaccurate prediction of the energies of the excited states. The states occupied in the ground state (and hence the Hellmann-Feynman forces used to determine the atomic structure) are not affected by the gap problem. The sharpness of the edges of the *s* and *p* bands is certainly a surprising result. If we consider that the technique used for performing the Brillouin-zone integrations involves a small smearing of the one-electron states, we have to conclude that the band edges are sharply defined, even if we superpose the results obtained from a number of independent atomic configurations.

The analysis of the partial DOS shows that even at the highest densities, the partial DOS of the empty states is essentially *p*-like. The form of the *s* band at higher binding energies is strongly influenced by the *s*-*d* hybridization. At densities lower than the M/NM transition, the states above E_F have pure *p* character. The DOS of the occupied states has *s* and *d* character, the small remaining *p* contribution is not due to *p* states inside the atomic sphere, but arises mainly from the overlap of *s* states centered on neighboring sites. This indicates that the M/NM transition is a band-crossing transition involving the *s* and *p* valence bands. Here again it is important to point at substantial differences between the electronic structure of the liquid and that of the crystalline reference configurations. As already pointed out by Mattheis

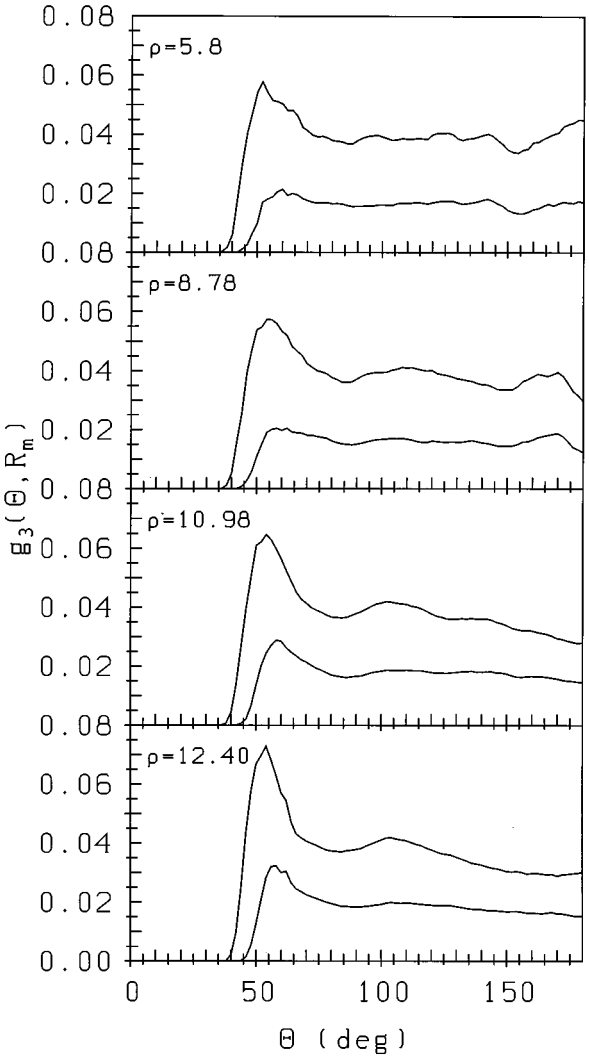

FIG. 7. Integrated bond angle distribution functions $g_3(\theta, R_m)$ for a maximum bond length $R_m = 4.0$ Å (upper line in each pannel) and $R_m = 3.5$ Å(lower lines in each panel), calculated at four different states along the liquid/vapor coexistence curve.

and Warren,[22] all crystalline structures show appreciable *s*-*p* hybridization in the valence and conduction bands even at the low densities where the gap begins to open, in contrast to the nearly pure *p* character of the conduction band in the liquid. That the liquidlike disorder leads to a reduction of the *s*-*p* hybridization is not a peculiarity of liquid Hg. In our studies of liquid Ge (Refs. 29 and 45) we have shown that structural disorder leads to a strongly reduced *s*-*p* mixing compared to all crystalline forms of Ge (including the high-pressure metallic polymorphs) and further to the formation of a deep pseudogap in the middle of the valence band separating subbands of dominant *s* and *p* character, respectively. This is also confirmed by detailed photoemission studies.[25]

C. Electron localization

Of particular interest is the character of the states (localized or extended) close to the Fermi energy. From the eigen-

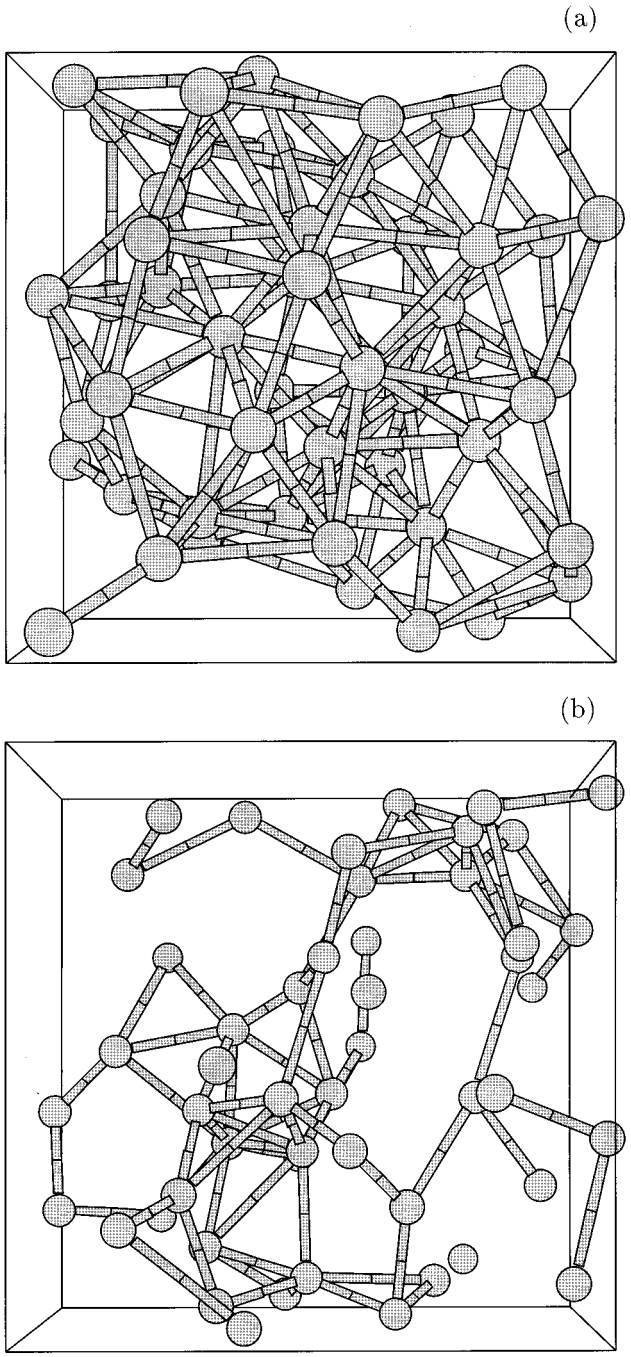

FIG. 8. Characteristic instantaneous configurations of the Hg ensemble at (a) the highest and (b) lowest densities considered in this study. Nearest-neighbor bonds shorter than 4 Å are drawn as solid bars.

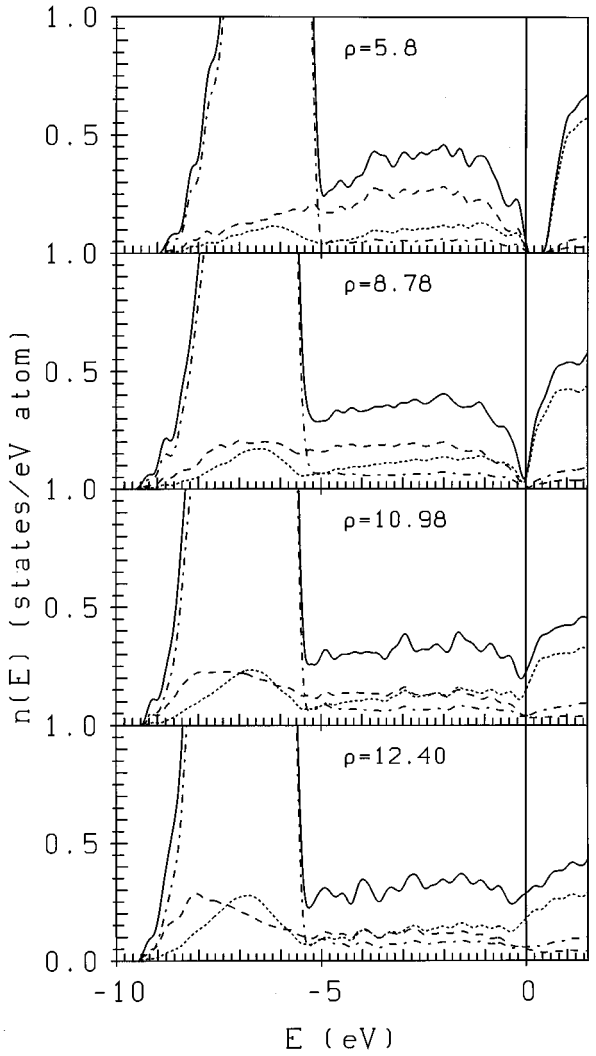

FIG. 9. Electron density of states $n(E)$ for liquid mercury, calculated for four different states along the coexistence curve (densities are given in g cm^3). Full curve, total DOS; dashed, dotted, and dash-dotted lines, s, p, and d partial DOS's, respectively. The large intensity between 9 and 5 eV binding energy is due to the 5d band. Note the gradual formation of a band gap at the Fermi level. See the text.

states decomposed by projecting the individual plane-wave components onto spherical waves inside the atomic spheres, we can calculate the participation ratio[46] p_i of the eigenstates ψ_i with energies E_i according to

$$p_i=\left(\sum_{j,l}|e_{i,l}(\vec{R}_j)|^2\right)^2\left(N\sum_{j,l}|e_{i,l}(\vec{R}_j)|^4\right)^{-1}$$

where the sum runs over the angular-momentum components l at all atomic sites $\vec{R}_j$. With this definition, $p_i\sim 1$ for extended and $p_i\sim N^{-1}$ for localized states. Figure 10 shows the distribution of the participation ratios of the eigenstates. The important result is that all states in the s,p valence bands are extended. A tendency towards localization exists only at both edges of the d band. In the s,p band a weak trend to lower values of the participation ratio is found only very close to the critical point. This is the central result of our study: in fluid mercury expansion leads to a narrowing of the s and p bands and finally to a M/NM transition of the band-crossing type. However, the band edges remain well defined even at the lowest densities and highest temperatures, we find no indication for a pronounced tailing of the bands, nor for a localization of the states at the upper edge of the valence or the lower edge of the conduction band. This would seem to suggest that the M/NM transition is a simple band crossing transition and that Anderson localization plays only

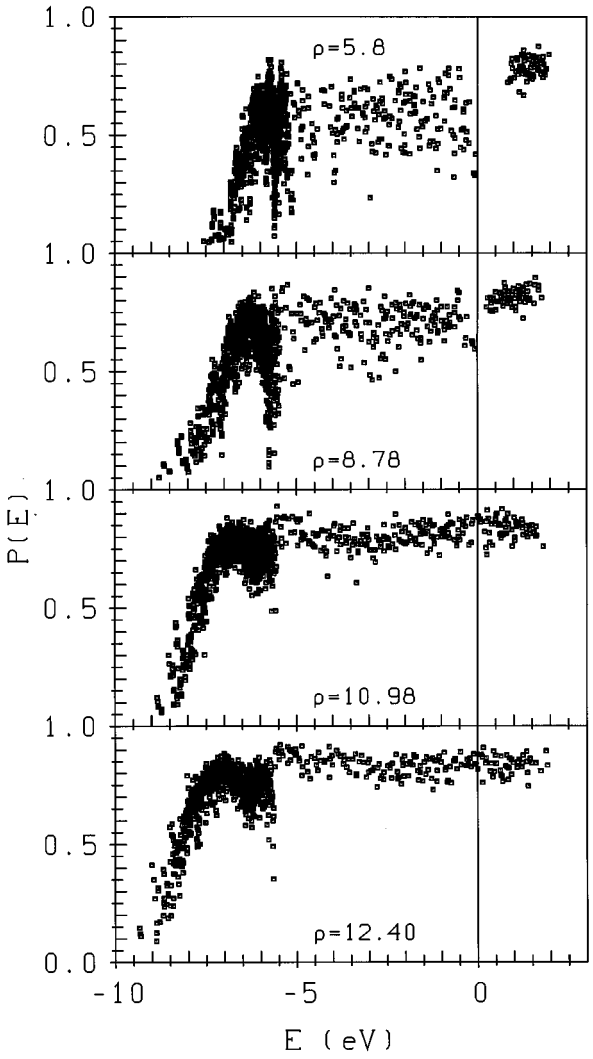

FIG. 10. Distribution of the participation ratio p_i of the electronic eigenstates ψ_i of expanded fluid mercury at three different densities. $p_i \sim 1$ corresponds to extended and $p_i \sim N^{-1}$ to localized states.

a minor role. This conclusion is also supported by the comparison of our results for the opening of the s,p gap and of the optical data of Yao *et al.*[6] with the conductivity data of Hefner *et al.*[5] This comparison shows that there is no essential difference between a mobility gap and the optical gap and hence agrees with our band-crossing scenario for the transition.

VI. DISCUSSION AND CONCLUSIONS

In summary, we have presented detailed *ab initio* LDF studies of the variation of the atomic and electronic structure of expanded liquid Hg along the liquid-vapor coexistence curve, from the triple point to close to the critical point. Our results for the atomic structure are in excellent agreement with experiment, even at the lowest densities and highest temperatures. We find that the expansion induces only a small change in the nearest-neighbor distance, but leads to a reduction of the nearest-neighbor coordination numbers and a wider fluctuation of the nearest-neighbor geometries. At the lowest densities close to the M/NM transition and to the critical point rather compact clusters with relatively high coordination numbers coexist with dilute regions where the coordination numbers are very low. Our results are in essential agreement with a recently proposed atomic scenario[15] for the M/NM transition in terms of metallic clusters of decreasing size and loosening connectivity. For the electronic structure we find a progressive deepening of the pseudogap at the Fermi level and the opening of a real gap at precisely the same density where both optical data[6] and conductivity measurements[5] locate the M/NM transition. Surprisingly, the band edges remain sharp and we do not find any indication for a localization of states close to the band edges. The comparison with the electronic densitities of states of expanded crystalline structures with comparable densities shows that the absence of long-range order is rather important for understanding the form of the bands. Note that the DOS of a Bethe lattice (or Cayley tree), i.e., of a structure that is characterized solely by a mean interatomic distance and coordination number and where all further translational or orientational correlations are absent, is semielliptic with sharp band edges.

Our results suggests that the M/NM transition is simply a band-crossing transition and that both disorder-induced localization and many-body effects might be less important for describing the transition than has been assumed in current scenarios for the transition. Of course we cannot exclude that localization occurs on clusters that are even larger than the dimensions of our models. However, this would mean that a conductivity gap appears before the optical gap opens, and this would contradict not only our LDF results, but also experiment.

Similarly, our LDF calculations do not allow us to draw any direct conclusions about the possible importance of many-body correlations. However, simple arguments suggest that correlation might be less important than assumed up to now. In general the LDA tends to underestimate the width of the gap. Hence the LDA error would place the M/NM transition at lower rather that at higher densities. A calculation considering correlation effects (e.g., LDA plus Hubbard-type Coulomb interactions) could only shift the onset of the gap to even higher densities and hence lead to poorer agreement with experiment. But, of course, further studies of other physical properties (e.g., Knight shift, and magnetic susceptibility) on the basis of our LDF results will be necessary to further support the description of the M/NM transition as a simple band-crossing transition. Finally we want to emphasize that the present results on Hg should not be used to make any extrapolations concerning the M/NM transition in the expanded alkali metals where the gap opens in the middle of the half-filled conduction band and where the band-crossing scenario is clearly inappropriate.

ACKNOWLEDGMENT

This work has been supported by Siemens-Nixdorf Austria within the framework of the Supercomputing Cooperation with the Technische Universität Wien.

[1] W. Freyland and F. Hensel, in *The Metallic and the Nonmetallic States of Matter*, edited by P. P. Edwards and C. N. R. Rao (Taylor and Francis, London, 1985), p. 93; F. Hensel and H. Uchtmann, Annu. Rev. Phys. Chem. **40**, 61 (1989).
[2] F. Hensel and U. Frank, Ber. Bunsenges. Phys. Chem. **70**, 1154 (1966).
[3] M. Yao and H. Endo, J. Phys. Soc. Jpn. **51**, 966 (1982); **51**, 1504 (1982).
[4] U. Even and J. Jortner, Phys. Rev. B **8**, 2536 (1973).
[5] W. Hefner, R. W. Schmutzler, and F. Hensel, J. Phys. (Paris) Colloq. **41**, C8-62 (1980).
[6] M. Yao, W. Hayami, and H. Endo, J. Non-Cryst. Solids **117/118**, 473 (1990).
[7] U. El-Hanany and W. W. Warren, Phys. Rev. Lett. **34**, 1276 (1975).
[8] S. Jüngst, B. Knuth, and F. Hensel, Phys. Rev. Lett. **55**, 2160 (1985).
[9] K. Tamura and S. Hosokawa, J. Non-Cryst. Solids **156-158**, 646 (1993); Proceedings of the Ninth International Conference on Liquid and Amorphous Metals, Chicago, 1995 [J. Non-Cryst. Solids **205-207**, 239 (1996) and references cited therein].
[10] K. Suzuki, M. Inutake, S. Fujiwaka, M. Yao, and H. Endo, J. Phys. (Paris) Colloq. **41**, C8-66 (1980).
[11] B. Widom and J. S. Rowlinson, J. Chem. Phys. **52**, 1670 (1970).
[12] P. C. Hemmer and G. Stell, Phys. Rev. Lett. **24**, 1784 (1970).
[13] N. D. Mermin, Phys. Rev. Lett. **26**, 957 (1971).
[14] R. D. Goldstein and N. W. Ashcroft, Phys. Rev. Lett. **55**, 2164 (1985).
[15] M. Ross and F. Hensel, J. Phys. Condens. Matter **8**, 1909 (1996).
[16] S. Nagel, R. Redmer, and G. Röpke, Proceedings of the Ninth International Conference on Liquid and Amorphous Metals, Chicago, 1995 [J. Non-Cryst. Solids **205-207**, 247 (1996)].
[17] N. F. Mott, Philos. Mag. **13**, 989 (1966); **26**, 505 (1972); *Metal-Insulator Transitions* (Taylor and Francis, London, 1974).
[18] M. H. Cohen and J. Jortner, Phys. Rev. Lett. **30**, 696 (1973); Phys. Rev. A **10**, 978 (1974).
[19] L. A. Turkevich and M. H. Cohen, Phys. Rev. Lett. **53**, 2323 (1984).
[20] M. A. C. Devillers and R. G. Ross, J. Phys. F **5**, 73 (1975).
[21] M. Overhof, H. Uchtmann, and F. Hensel, J. Phys. F **6**, 523 (1976).
[22] L. F. Mattheis and W. W. Warren, Phys. Rev. B **16**, 624 (1977).
[23] F. Yonezawa and F. Martino, Solid State Commun. **18**, 1471 (1976); F. Yonezawa, Y. Ishida, F. Martino, and S. Asano, in *Liquid Metals 1976*, edited by R. Evans and D. A. Greenwood (The Institute of Physics, London, 1977), p. 385.
[24] W. Jank and J. Hafner, Phys. Rev. B **42**, 6926 (1990).
[25] G. Indlekofer, P. Oelhafen, R. Lapka, and H. J. Güntherodt, Z. Phys. Chem. **157**, 465 (1988).
[26] R. Car and M. Parrinello, Phys. Rev. Lett. **55**, 2471 (1985).
[27] M. C. Payne, M. P. Teter, D. C. Allan, T. A. Arias, and J. D. Joannopoulos, Rev. Mod. Phys. **64**, 1045 (1994).
[28] G. Kresse and J. Hafner, Phys. Rev. B **47**, 558 (1993); **48**, 13 115 (1993).
[29] G. Kresse and J. Hafner, Phys. Rev. B **49**, 14 251 (1994).
[30] G. Kresse and J. Furthmüller, Comput. Mater. Sci. **6**, 15 (1996).
[31] G. Kresse and J. Furthmüller, Phys. Rev. B **54**, 11 169 (1996).
[32] M. Methfessel and A. Paxton, Phys. Rev. B **40**, 3616 (1989).
[33] D. Vanderbilt, Phys. Rev. B **41**, 7892 (1990).
[34] G. Kresse and J. Hafner, J. Phys.: Condens. Matter **6**, 8245 (1994).
[35] R. D. van Zee, S. C. Blankespoor, and T. S. Zwier, J. Chem. Phys. 88, 4650 (1988).
[36] P. Ballone and G. Galli, Phys. Rev. B **42**, 1112 (1990).
[37] J. P. Perdew, J. A. Chevary, S. H. Vosko, K. A. Jackson, M. R. Pedersen, D. J. Singh, and C. Fiolleais, Phys. Rev. B **46**, 6671 (1992).
[38] O. Schulte and W. B. Holzapfel, Phys. Rev. B **48**, 14 009 (1993).
[39] P. Villars and L.D. Calvert, *Pearson's Handbook of Crystallographic Data for Intermetallic Phases* (ASM International, Metals Park, OH, 1991).
[40] G. Kresse, J. Furthmüller, and J. Hafner, Phys. Rev B **50**, 13 181 (1994).
[41] K. Seifert, J. Hafner, J. Furthmüller, and G. Kresse, J. Phys. Condens. Matter **7**, 3683 (1995).
[42] Y. Waseda, *The Structure of Non-crystalline Materials — Liquids and Amorphous Solids* (McGraw-Hill, New York, 1980).
[43] G. Kahl, J. Non-Cryst. Solids **156-158**, 15 (1993).
[44] A. Eichler, J. Hafner, G. Kresse, and J. Furthmüller, Surf. Sci. **346**, 300 (1996).
[45] W. Jank and J. Hafner, Phys. Rev. B **41**, 1497 (1990).
[46] R. J. Bell and P. Dean, in *Amorphous Materials*, edited by R. W. Douglas and B. Ellis (Wiley, New York, 1972), p. 443.
[47] M. Atoji, J. E. Schirber, and C. A. Swenson, J. Chem. Phys. **31**, 1628 (1959).